Atomic control of layer-by-layer epitaxial growth on $SrTiO_3(001)$: Molecular-dynamics simulations

Momoji Kubo, Yasunori Oumi, Ryuji Miura, Andras Stirling,* and Akira Miyamoto†
Department of Molecular Chemistry and Engineering, Faculty of Engineering, Tohoku University, Aoba-ku, Sendai 980-77, Japan

Masashi Kawasaki, Mamoru Yoshimoto, and Hideomi Koinuma
Materials and Structures Laboratory, Tokyo Institute of Technology, Midori-ku, Yokohama 226, Japan
(Received 5 December 1996; revised manuscript received 1 May 1997)

Molecular-dynamics simulations were performed to clarify the structures of SrO and BaO layers on a $SrTiO_3(001)$ substrate at the atomic level, and to predict an appropriate buffer layer for $YBa_2Cu_3O_{7-x}/SrTiO_3$ heterojunction. The atomic structure of these layers grown on a $SrTiO_3(001)$ substrate terminated on the TiO_2 atomic plane was investigated. From the analysis of the angle distribution of Sr-O-Sr and the radial distribution between Sr and O, the first single SrO layer on the $SrTiO_3(001)$ substrate was found to keep a perfect NaCl-type structure. However, the structure of the second SrO layer deviated from a NaCl-type structure. This result suggests that only a single SrO layer is able to grow epitaxially and uniformly on the $SrTiO_3(001)$ substrate terminated on the TiO_2 atomic plane. Since a BaO layer is one component of the $YBa_2Cu_3O_{7-x}$ layered structure, a detailed understanding of the $BaO/SrTiO_3(001)$ heterojunction has been desired. Here, the stress induced by the lattice mismatch of the $BaO/SrTiO_3(001)$ and $BaO/SrO/SrTiO_3(001)$ heterojunction was evaluated. The $BaO/SrTiO_3(001)$ gained 1.2 GPa stress, while surprisingly the $BaO/SrO/SrTiO_3(001)$ did not have any stress. Moreover, the BaO layer was found to grow epitaxially and uniformly on the $SrO/SrTiO_3(001)$. Note that $YBa_2Cu_3O_{7-x}$ is expected to grow epitaxially on a BaO layer since the BaO layer is a part of the $YBa_2Cu_3O_{7-x}$ layered structure. Hence, we suggest that BaO/SrO is a suitable buffer layer for the $YBa_2Cu_3O_{7-x}/SrTiO_3$ heterojunction. [S0163-1829(97)03343-2]

I. INTRODUCTION

Technology on the artificial construction of atomically defined metal oxide layers has been desired in relation to electronic, magnetic, and optical devices as well as other advanced materials such as supported metal oxide catalysts.[1–7] Specifically, a two-dimensional and epitaxial ultrathin oxide layer with atomically flat surface is essential for the development of oxide-based heterojunction devices such as Josephson tunnel junctions. $SrTiO_3(001)$ has attracted much attention among metal oxide crystals, due to its significance as a lattice-matched substrate suitable for the epitaxial growth of high-T_c superconducting films. Hence, the epitaxial growth process and atomic surface structure of $SrTiO_3$ have been extensively investigated using various experimental techniques, such as laser molecular beam epitaxy (laser MBE), Auger electron spectroscopy, reflection high-energy electron diffraction (RHEED), low-energy electron diffraction, x-ray photoelectron spectroscopy, x-ray photoelectron diffraction, coaxial impact collision ion-scattering spectroscopy (CAICISS), atomic force microscopy (AFM), and scanning tunneling microscopy.[8–14]

Recently, Kawasaki and co-workers[14] succeeded in fabricating an atomically flat and smooth $SrTiO_3(001)$ surface completely terminated on the TiO_2 atomic plane by NH_4F-HF treatment. The $SrTiO_3(001)$ surface treated by the above technique is expected to enable atomically regulated epitaxy of oxides comparable to that of semiconductors, and to realize the Josephson tunnel junction. Moreover, those flat and smooth $SrTiO_3(001)$ substrates enable us the atomistic design of high-T_c superconducting film/$SrTiO_3(001)$ heterojunction. Especially since $SrTiO_3$ has a structure similar to $YBa_2Cu_3O_{7-x}$ (YBCO), and the lattice mismatch is less than 2%, $SrTiO_3$ is expected to serve as insulator thin films and substrates for the Josephson tunnel junction based on YBCO. Although the epitaxial growth process of YBCO on a $SrTiO_3(001)$ surface has been investigated,[1–3] the fabrication of the Josephson tunnel junction has not been achieved. Hence, the detailed understanding of the interface structure between YBCO and $SrTiO_3$ substrate, and the design of a suitable buffer layer for a $YBCO/SrTiO_3(001)$ heterojunction on an atomic level are desired. Particularly, the interface structure as well as the epitaxial growth process of BaO thin film on $SrTiO_3$ surfaces are interesting, since the BaO layer is one component of the YBCO layered structure. On the other hand, the structure of a $BaO/SrTiO_3(001)$ heterojunction gained much recent attention, because Tabata and coworkers recently reported that the $BaTiO_3/SrTiO_3$ superlattice has tremendous dielectric properties.[15,16]

Although much information has been experimentally obtained for the homojunctions and heterojunctions on a $SrTiO_3$ substrate, theoretical approaches, such as molecular dynamics (MD), quantum chemistry, Monte Carlo simulation, and computer graphics (CG) would be also desirable. Interesting theoretical and computational studies have been done to elucidate details of the surface reconstruction, electronic structure, dielectric property, ferroelectricity, phonon frequencies, band structure, and energetics of $SrTiO_3$.[17–24] However, few works were devoted to the interface structure of the oxide/$SrTiO_3$ heterojunction.[25] The effect of the ter-

TABLE I. The potential parameters of Sr, Ba, Ti, and O atoms.

Atom	Z_i	a_i (Å)	b_i (Å)
Sr	+1.2	1.506	0.070
Ba	+1.2	1.666	0.070
Ti	+2.4	1.109	0.070
O	−1.2	1.503	0.075

mination of the atomic plane of the $SrTiO_3(001)$ surface on the above heterojunction structures should be clarified, since two different surface terminations, with either SrO or TiO_2, are possible. We applied MD technique to investigate the atomic structure of the $SrO/SrTiO_3(001)$ and $BaO/SrTiO_3(001)$ heterointerfaces as well as the effect of surface termination of the $SrTiO_3(001)$ substrate on the above interface structure. Furthermore, an adequate buffer layer for the fabrication of the ideal $BaO/SrTiO_3(001)$ heterojunction is suggested to realize the $YBCO/SrTiO_3(001)$ Josephson tunnel junction.

II. METHOD

MD simulations were carried out with the MXDORTO program developed by Kawamura.[26] The Verlet algorithm[27] was used for the calculation of the atomic motions, while the Ewald method[28] was applied for the calculation of the electrostatic interactions. We used periodic boundary conditions. Temperature was controlled by means of scaling the atom velocities. The calculations were performed for 10 000 steps with a time step of 2.0×10^{-15} s. The two-body, central force, interatomic potential, shown in Eq. (1), was used for all calculations. In Eq. (1), the first and second terms refer to Coulomb and exchange repulsion interactions, respectively,

$$u(r_{ij})=Z_iZ_je^2/r_{ij}+f_0(b_i+b_j)\exp[(a_i+a_j-r_{ij})/(b_i+b_j)]. \quad (1)$$

Z_i is the atomic charge, e the elementary electric charge, r_{ij} the interatomic distance, and f_0 a constant. The parameters a and b represent the size and stiffness, respectively, in the exchange repulsion interaction.

In order to simulate the epitaxial growth process of a SrO layer on a $SrTiO_3(001)$ substrate, we employed our crystal growth MD simulator.[29,30] We note that the homoepitaxial growth process of MgO(001) has been successfully simulated using the above MD code.[29] The detailed algorithm of the MD code is described in Refs. 29 and 30.

Calculations were performed on Hewlett Packard Apollo 9000 Model 712/60 workstation, while the CG visualization was made with an Insight II software of MSI (Ref. 31) on a Silicon Graphics IRIS-Indigo2 workstation. Dynamic features of the atoms were also investigated by using real-time visualization with the MOMOVIE code and RYUGA (Ref. 32) code developed in our laboratory on OMRON LUNA-88K workstation and Hewlett Packard Apollo 9000 Model 715/33 workstation, respectively.

TABLE II. Lattice constants of $SrTiO_3$, SrO, BaO, and $BaTiO_3$ crystals derived from the MD simulations.

	MD simulation (Å)	Experimental result (Å)
$SrTiO_3$	3.905±0.002	3.905
SrO	5.160±0.004	5.160
BaO	5.523±0.004	5.523
$BaTiO_3$	3.982±0.002	4.012

TABLE III. Expansion coefficients of $SrTiO_3$, SrO, BaO, and $BaTiO_3$ crystals derived from the MD simulations.

	MD simulation	Experimental result
$SrTiO_3$	1.04×10^{-5}/K	1.04×10^{-5}/K
SrO	1.39×10^{-5}/K	1.52×10^{-5}/K
BaO	1.93×10^{-5}/K	1.86×10^{-5}/K
$BaTiO_3$	1.22×10^{-5}/K	1.2×10^{-5}/K

III. RESULTS AND DISCUSSION

A. Development of force field for $SrTiO_3$, SrO, and BaO

The accurate force field for the $SrTiO_3$ substrate is required for the present purpose. The potential parameters for $SrTiO_3$ in Eq. (1) were determined by using MD simulations, as they reproduce various properties of $SrTiO_3$ crystal. The determined potential parameters of Sr, Ti, and O atoms are presented in Table I. The calculated lattice constant and expansion coefficient of $SrTiO_3$ crystal, shown in Tables II and III, respectively, are in good agreement with the experimental results.[33,34] The trajectories of Sr, Ti, and O atoms in the $SrTiO_3$ crystal were also close to the average positions of the ions determined by the x-ray diffraction (XRD) technique.[33] Moreover, the mean-square displacements (MSD) of Sr, Ti, and O atoms from the positions derived by the XRD were 0.014, 0.004, and 0.012 Å^2, respectively. These MSD values are not significant in comparison of the temperature factor in the XRD analysis. The calculated lattice constant and expansion coefficient of SrO crystal, shown in Tables II and III, respectively, also agree with the experimental results.[33,35] The MSD of Sr and O atoms in bulk SrO during 10 000 time steps in MD simulations at several temperatures were calculated (Table IV). Although the MSD value increased gradually with increasing temperature below 2400 K, noticeably large MSD values were suddenly observed at 2500 K. This indicates that the simulated SrO crystal melted at around 2500 K. This agrees with the experimental melting point of 2703 K.[36]

TABLE IV. The mean square displacements (MSD) of atoms in SrO bulk during 10 000 time steps with increasing temperature.

Temperature (K)	MSD(Sr) (Å^2)	MSD(O) (Å^2)
300	0.016	0.017
1000	0.069	0.070
1500	0.118	0.120
2000	0.193	0.193
2400	0.233	0.615
2500	106.078	87.526

TABLE V. The mean square displacements (MSD) of atoms in BaO bulk during 10 000 time steps with increasing temperature.

Temperature (K)	MSD(Ba) (Å^2)	MSD(O) (Å^2)
300	0.024	0.024
1000	0.081	0.078
1500	0.167	0.161
2000	0.229	0.225
2100	0.261	0.254
2200	72.404	85.220

The force field for BaO was constructed for the simulation of the BaO/$SrTiO_3$(001) heterointerface structure. The determined potential parameters of the Ba atom are presented in Table I. The same potential parameters of O as for $SrTiO_3$ and SrO were employed for the BaO force field. The calculated lattice constant and expansion coefficient of BaO crystal, shown in Tables II and III, respectively, are in good agreement with the experimental results.[33] The positions of the ions in the BaO crystal determined by the XRD were also reproduced by the MD simulations.[33] The MSD of Ba and O atoms in bulk BaO during 10 000 time steps in MD simulations at several temperatures are shown in Table V, indicating that the simulated BaO crystal melted at around 2200 K. This agrees with the experimental melting point of 2191 K.[36] The calculated lattice constant and expansion coefficient for $BaTiO_3$ crystal, also shown in Tables II and III, respectively, are also found to be in good agreement with the experimental results.[33,37]

B. Epitaxial growth process of a SrO layer on $SrTiO_3$(001) terminated by TiO_2 atomic plane

Our crystal growth MD simulator and new force field were applied to the investigation of the epitaxial growth process of a SrO thin layer on a $SrTiO_3$(001) surface. Since the $SrTiO_3$ crystal has a structure stacked alternately by nonpolar SrO and TiO_2 atomic plane [Fig. 1(a)], two different surface terminations by either SrO or TiO_2 at the (001) top layer are possible [Figs. 1(b) and 1(c)]. Yoshimoto and co-workers[13] determined the structure of the topmost plane of $SrTiO_3$(001) surface by means of CAICISS measurements. They revealed that the $SrTiO_3$(001) surface of as-supplied substrates as well as O_2-annealed substrates was predominantly terminated on the TiO_2 atomic planes. To be able to compare with the experimental results,[14,38] we examined the $SrTiO_3$(001) surface terminated on the TiO_2 in our MD simulations.

In the epitaxial growth simulation, a total of 32 SrO molecules are emitted one by one at regular time intervals of 1000 time steps with constant velocity of 900 m/s. The amount of SrO molecules is equal to the number of Sr and O atoms which make a single SrO layer on the $SrTiO_3$, in the MD unit cell. Figure 2 shows results at 700 K. $SrTiO_3$ substrate is represented by atomic bonds, while deposited SrO molecules are represented by spheres. Surprisingly, after 50 000 time steps, a two-dimensional (2D) epitaxial SrO thin layer without any defects was observed. The deposited SrO molecules continued the perovskite structure and (001) oriented configuration during the MD simulation.

Kawasaki and co-workers[38] applied laser MBE to fabricate a SrO layer on the $SrTiO_3$(001) substrate. They used an atomically flat and smooth $SrTiO_3$(001) substrate terminated on the TiO_2 obtained by a buffered NH_4F-HF treatment.[14] They achieved the epitaxial and 2D growth of a single SrO layer at around 700 K, in good agreement with our simulation results. Specifically, at around 700 K they observe[38] a RHEED oscillation when a single SrO layer grew on the atomically flat $SrTiO_3$(001) surface terminated on the TiO_2. Moreover, they confirmed atomic flatness of the grown SrO layer on the substrate with an AFM.

C. Atomic structure of a topmost single SrO layer of SrO/$SrTiO_3$(001) and SrO/SrO/$SrTiO_3$(001)

Given the results above, in the present section we assumed that two-dimensionally flat and smooth SrO layers are constructed on the $SrTiO_3$(001) substrate terminated on the TiO_2 atomic plane. We employed two different models to analyze the atomic structure of the grown SrO layers on the $SrTiO_3$(001) substrate. In model (a), a single SrO layer is stacked on the $SrTiO_3$(001) substrate, and the structure of this SrO layer was examined. In model (b), two SrO layers are stacked on the $SrTiO_3$(001) substrate, and the structure of the topmost single SrO layer was investigated. We focused on the difference between the atomic structure of the first SrO layer [model (a)] and the second SrO layer [model (b)]. The structure in model (a) is identical to that of the $SrTiO_3$(001) substrate terminated on the SrO atomic plane, while the structure in model (b) is identical to that of a single

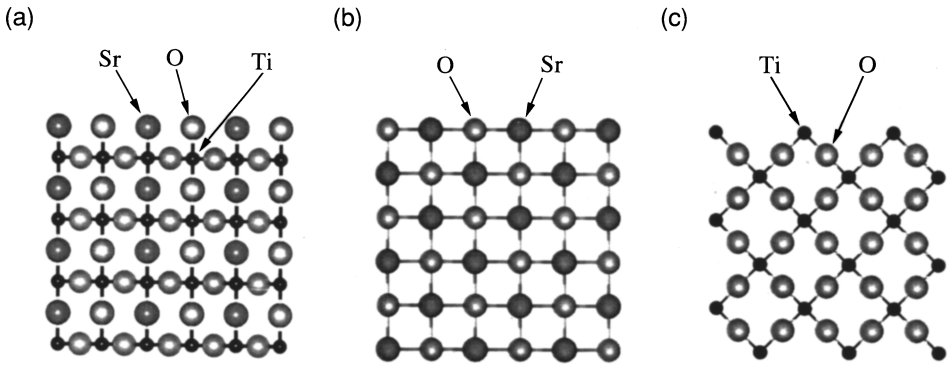

FIG. 1. Computer graphics pictures of (a) $SrTiO_3$ crystal, (b) SrO atomic plane of $SrTiO_3$, and (c) TiO_2 atomic plane of $SrTiO_3$.

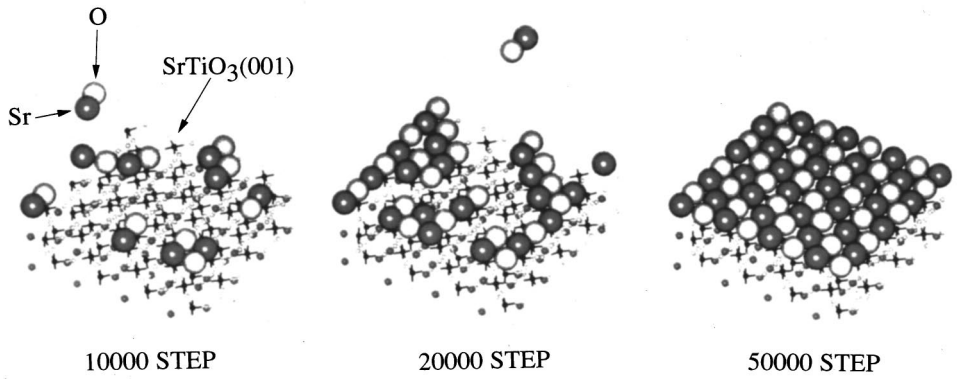

FIG. 2. Epitaxial growth process of a single SrO layer on $SrTiO_3(001)$ terminated on the TiO_2 atomic layer at 700 K.

SrO layer on the $SrTiO_3(001)$ substrate terminated on the SrO atomic plane. In the present section, all MD calculations were carried out at 300 K.

We analyzed the Sr-O-Sr angle distribution function in the topmost single SrO layer of models (a) and (b), during 10 000 MD time steps (Fig. 3). A single strong peak is obtained at almost 90° in the angle distribution function for both cases. This result suggests that the topmost SrO layer of both models (a) and (b) keeps an NaCl-type structure. However, a small difference in the peak shape (i.e., the width or standard deviation, and the tails) between the two models was observed. The Sr-O-Sr angle peak was distributed from 80° to 100° for model (a) and from 70° to 110° for model (b). Consequently, the peak height in model (b) is lower than that in model (a).

Furthermore, the radial distribution function between Sr and O in the topmost single SrO layer of both models (a) and (b) was investigated during 10 000 time steps (Fig. 4), in order to clarify the detailed difference of the topmost SrO structure of the two different models. Sharp peaks were obtained at 2.8, 6.2, 8.3, and 9.9 Å for model (a). A different radial distribution was observed for model (b). For example, the first peak of 2.8 Å in model (a) was replaced by two separated peaks of 2.6 and 3.8 Å in model (b). Similarly the second peak of 6.2 Å in model (a) was replaced by two separated peaks of 5.9 and 6.9 Å in model (b). The trend in the change of the peak position is similar to that of the first peak. The third peak was also replaced by two peaks. Other peaks are missing in model (b). These results indicate that the topmost SrO layer of model (a) keeps an NaCl-type structure, while that of model (b) is slightly deviated from a perfect NaCl-type structure.

The schematic structure of the topmost single SrO layers of models (a) and (b) is shown in Figs. 5(a) and 5(b), respectively, as predicted by the present MD calculations. The origin of the above different SrO structures is interpreted as follows. Since the single topmost SrO layer of model (a) is directly attached to the TiO_2 atomic plane, the topmost single

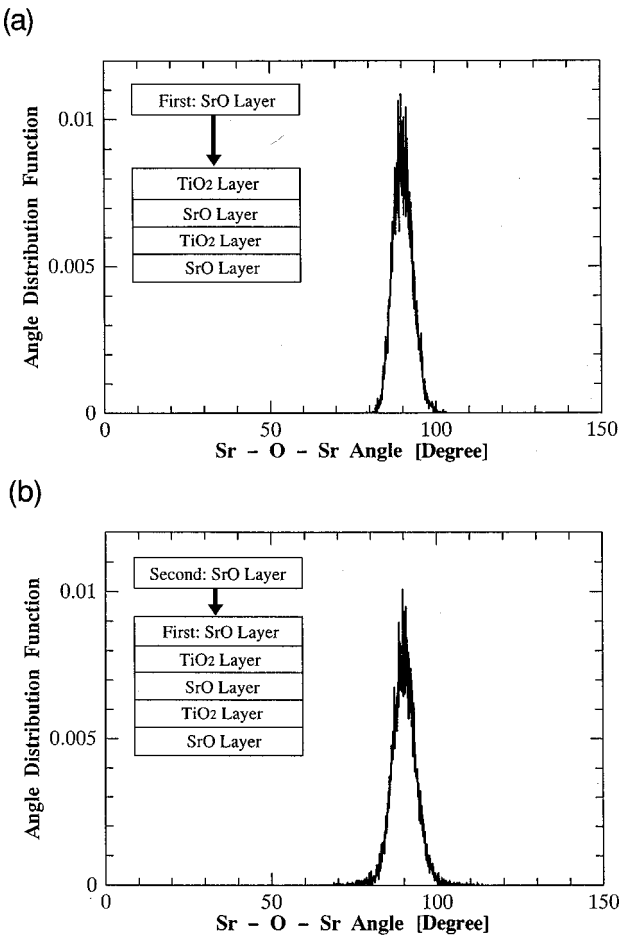

FIG. 3. Angle distribution function of Sr-O-Sr in a topmost single SrO layer of models (a) and (b).

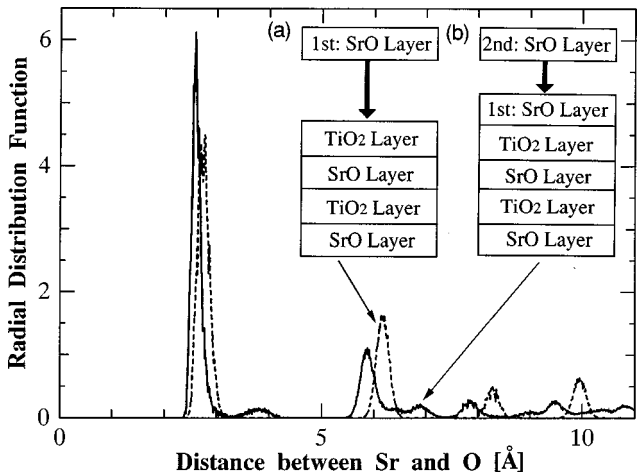

FIG. 4. Radial distribution function between Sr and O in a topmost single SrO layer of models (a) and (b).

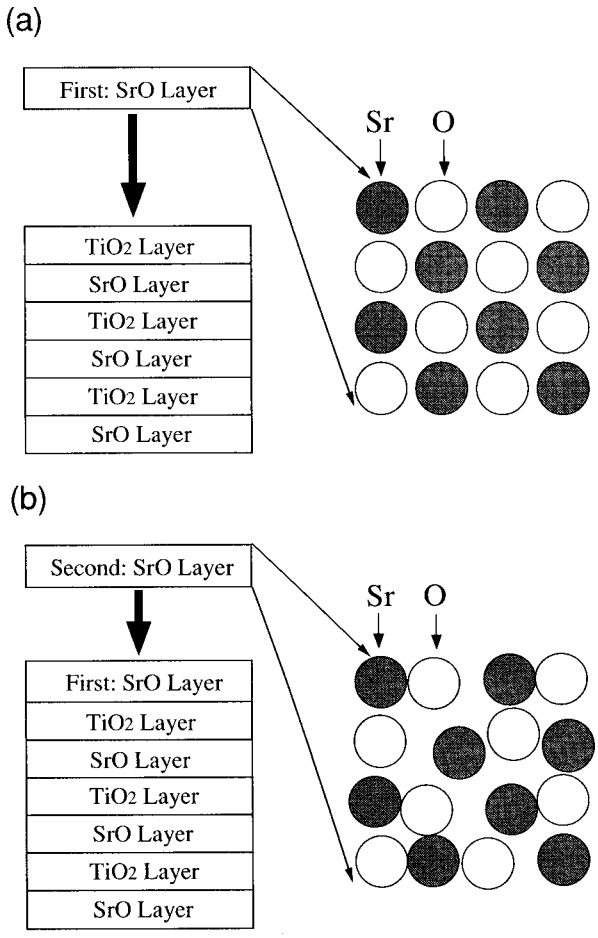

FIG. 5. Schematic of the structure of a topmost single SrO layer in models (a) and (b), predicted by MD.

SrO layer was fabricated as a part of a $SrTiO_3$ crystal. On the other hand, since the second SrO layer of model (b) is directly attached to the SrO atomic plane, the topmost second SrO layer was constructed as part of a SrO crystal instead of a $SrTiO_3$ crystal. Hence, we propose that only the first SrO layer inherits the structure of the $SrTiO_3$ crystal, and the second SrO layer has the nature of the SrO crystal on the $SrTiO_3(001)$ substrate terminated on the TiO_2 atomic plane. The lattice mismatch between $SrTiO_3$ ($a=3.905$ Å) and SrO ($1/\sqrt{2}a=3.649$ Å) crystals is responsible for the fluctuated structure of the second SrO layer in model (b), as shown in Fig. 5(b). Here, we compared the lattice constant of a $SrTiO_3$ crystal and the $1/\sqrt{2}$ lattice constant of a SrO crystal, because crystallographically, a SrO layer structure of the SrO crystal is tilted by 45° in comparison with that of the $SrTiO_3$ crystal as shown in Fig. 6. On the basis of the above discussion, the reason why the peak position of Sr-O radial distribution function in model (b) was ''divided'' into two peaks at the shorter distance and at the longer distance than that in model (a) is readily understandable (see Fig. 5). Since the lattice constant of the topmost SrO layer in model (b) is smaller than that of the $SrO/SrTiO_3$ substrate, some O atoms move slightly to positions closer to their neighbor Sr atoms and some Sr atoms also take similar movement. Hence, the distance between the O atom and the neighbor Sr atom decreases, while the distance between the O atom and another neighbor Sr atom increases.

We also calculated the atomic structure of the third and fourth SrO layers grown on the $SrTiO_3(001)$ substrate. They were also different from a perfect NaCl-type structure, similarly to that of the second SrO layer. Clearly, in our simulations only a single SrO layer can be grown epitaxially and uniformly on the $SrTiO_3(001)$ substrate terminated on the TiO_2 atomic plane.

Kawasaki and co-workers applied[38] the laser MBE technique to the formation of the SrO layers on the $SrTiO_3(001)$ substrate. They observed a single RHEED oscillation at first, as mentioned above; however no more RHEED oscillations were detected during the formation process of SrO layers on the $SrTiO_3(001)$ substrate. It indicates that only a single SrO is able to grow epitaxially and uniformly on the $SrTiO_3(001)$ substrate. This experimental result is in surprisingly good agreement with the present MD calculations.

D. Atomic structure of a topmost single BaO layer of $BaO/SrTiO_3(001)$ and $BaO/SrO/SrTiO_3(001)$

YBCO has attracted much attention because of its high-temperature superconductivity. Hence, growth, structure, interface, and superconducting properties of YBCO-based superlattices have been investigated extensively.[1–3] The fabrication of uniform $YBCO/SrTiO_3$ heterojunctions has been continuously studied because it is a main candidate for a Josephson tunnel junction material.[1–3] All the high-T_c su-

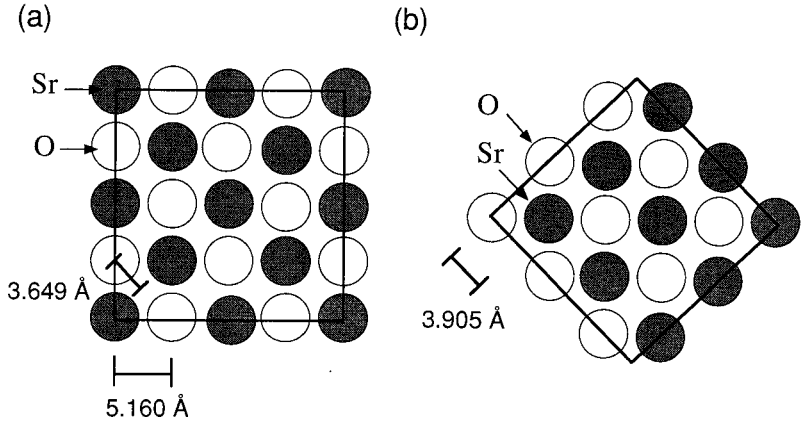

FIG. 6. Structure of the SrO atomic layer of (a) SrO crystal and (b) $SrTiO_3$ crystal as well as their lattice constants.

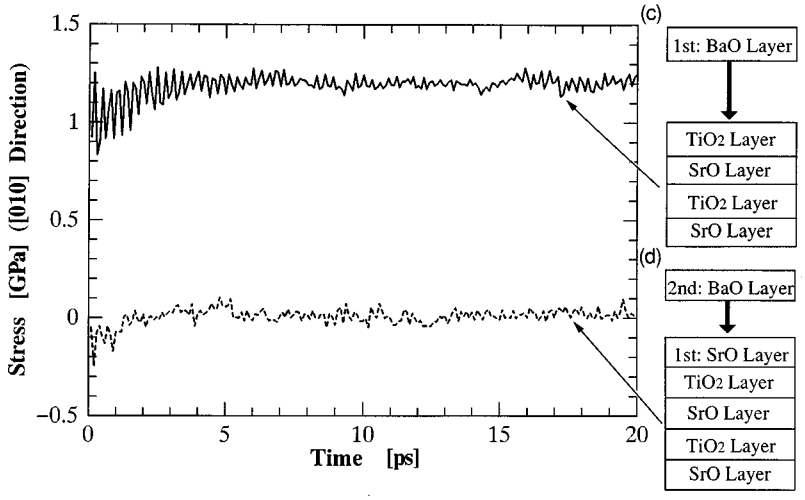

FIG. 7. [010] direction stress of a topmost single BaO layer in models (c) and (d) due to the lattice mismatch between layer and substrate.

perconductors have layered structure composed of alternating sequences of CuO_2 and other oxide layers. YBCO has a stacked structure of $BaO/CuO_2/Y/CuO_2/BaO/CuO$. In the present study, attention was given to the BaO layer.

We started with the $SrTiO_3(001)$ substrate terminated on the TiO_2 atomic plane, and assumed that a two-dimensionally flat and smooth BaO layer is grown on the $SrTiO_3(001)$ substrate, similarly to Sec. III C. We employed two different models to investigate the atomistic structure of the topmost single BaO layer on $SrTiO_3(001)$ substrate. In model (c), a single BaO layer is stacked on the $SrTiO_3(001)$ substrate terminated on the TiO_2 atomic plane. In model (d), a single BaO layer is stacked on a single SrO layer deposited on the $SrTiO_3(001)$ substrate terminated on the TiO_2 atomic plane. The single SrO layer is employed as a buffer layer for a $BaO/SrTiO_3(001)$ heterojunction. Since double, triple, and more SrO layers on the $SrTiO_3(001)$ substrate do not grow epitaxially, only a single SrO layer is employed as a buffer layer. The structure of model (d) is identical to that of a single BaO layer on the $SrTiO_3(001)$ substrate terminated on a SrO atomic plane. Generally, the fabrication of the heterojunction induces stress at the heterointerface because the substrate and constructed layers have different lattice constants. Thus, we focused on the difference between the stress at the heterointerface of models (c) and (d), as well as the atomic structure of the topmost single BaO layer. In the present section, all MD calculations were carried out at 300 K.

The time dependence of the [010] direction stress at the heterointerface of models (c) and (d) during 10 000 MD time steps is shown in Fig. 7. Model (c) kept approximately 1.2 GPa at the heterointerface, independent of the time. Surprisingly, in model (d), no stress was obtained due to the heterojunction. It is expected that the large stress in model (c) disturbs the subsequent fabrication of the uniform $YBCO/SrTiO_3(001)$ heterojunction. Hence, we proposed here that only a single SrO layer should be stacked on the $SrTiO_3(001)$ substrate terminated by TiO_2 atomic plane as a buffer layer to realize a regulated and uniform $BaO/SrTiO_3$ heterojunction.

The above result is interpreted as follows. Since the topmost single BaO layer in model (c) is directly attached to the TiO_2 atomic plane, and a $BaTiO_3$ crystal has also a stacked structure of alternating BaO and TiO_2 atomic planes, the BaO layer was fabricated as a part of a $BaTiO_3$ crystal. The lattice mismatch between the $SrTiO_3$ ($a=3.905$ Å) and $BaTiO_3$ ($a=4.012$ Å) crystals produces the above large stress, shown in Fig. 7. On the other hand, since the topmost single BaO layer in model (d) is directly attached to the SrO atomic plane, the topmost BaO layer was constructed as a part of a BaO crystal instead of a $BaTiO_3$ crystal. Furthermore, since the lattice constant of $SrTiO_3$ crystal ($a=3.905$ Å) is the same as that of BaO crystal ($1/\sqrt{2}a=3.905$ Å), model (d) did not gain any stress due to lattice mismatch, as shown in Fig. 7. Here, we compared the lattice constant of the $SrTiO_3$ crystal and the $1/\sqrt{2}$ lattice constant of the BaO crystal similarly to Sec. III C, because crystallographically a BaO layer structure of a BaO crystal, which has the same structure as a SrO crystal, is tilted by 45° compared with that of a $SrTiO_3$ crystal (see Fig. 6).

In order to confirm the validity of the single SrO buffer layer for a $BaO/SrTiO_3(001)$ heterojunction, the radial distribution function between Ba and O in the topmost single BaO layer of model (d) is compared to that between Sr and O

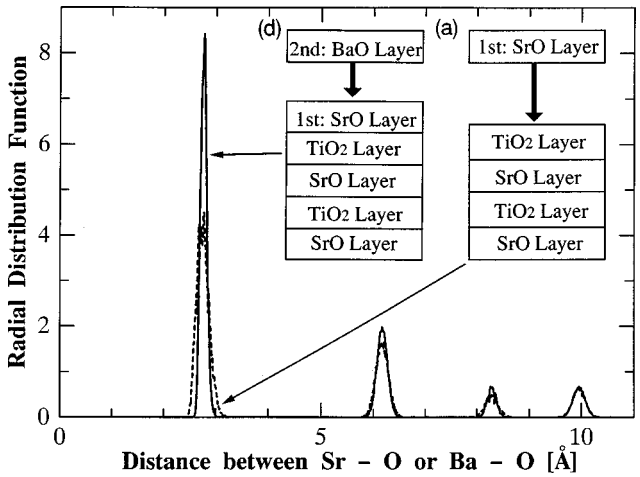

FIG. 8. Radial distribution function between Ba and O in a topmost single BaO layer in model (d). Radial distribution function between Sr and O in a topmost single SrO layer in model (a) is shown for comparison.

in the topmost single SrO layer of the $SrO/SrTiO_3(001)$ [model (a)]. The result is shown in Fig. 8. For both cases, the peaks were obtained at the same distances of 2.8, 6.2, 8.3, and 9.9 Å. This result is particularly surprising because the Ba-O distance in a BaO crystal ($a=5.523$ Å) is significantly different from the Sr-O distance in a SrO crystal ($a=5.160$ Å). From the analysis of Ba-O-Ba angle distribution and CG visualization, the BaO structure was found to keep a perfect NaCl-type structure, confirming that the BaO layer inherits the topmost SrO structure of the $SrO/SrTiO_3(001)$, i.e., an epitaxial and uniform single BaO layer is fabricated on the $SrO/SrTiO_3(001)$. Another two structures, $BaO/BaO/SrO/SrTiO_3(001)$ and $BaO/BaO/BaO/SrO/SrTiO_3(001)$, were simulated. The radial distribution function between Ba and O in the second and third BaO layers was similar to the that of the first BaO layer on the $SrO/SrTiO_3(001)$. Hence, we propose here that a number of BaO layers can be fabricated epitaxially and uniformly on the $SrO/SrTiO_3(001)$. This is directly related to the smaller stress observed at the $BaO/SrO/SrTiO_3(001)$ heterointerface.

Kawasaki and co-workers applied[38] laser-MBE to the formation of the BaO layers on the $SrTiO_3(001)$ terminated on the TiO_2 atomic plane and $SrO/SrTiO_3(001)$. They observed persistent RHEED oscillations during growth of the BaO layers on the $SrO/SrTiO_3(001)$, but not on the $SrTiO_3(001)$. These experimental results are in surprisingly good agreement with our MD calculations.

Finally, on the basis of the present MD simulations, we anticipated that YBCO, grows epitaxially on the BaO layer, since the BaO layer is part of the YBCO structure, and that (BaO layers/single SrO layer) are suitable buffer layers for the $YBCO/SrTiO_3$ heterojunction.

IV. CONCLUSION

The atomic structure of SrO and BaO layers grown on $SrTiO_3(001)$ substrate was elucidated via MD simulations. Furthermore, the suitable buffer layer for the $YBCO/SrTiO_3(001)$ heterojunction was predicted on the basis of the MD results. The interface structure of YBCO/BaO should be investigated to confirm our suggestion. If true, our prediction is certainly helpful for the design of the uniform and regulated $YBCO/SrTiO_3$ heterojunction. The combination of the present simulation method and experiments promises to aid in the artificial construction of atomically defined metal oxide layers.

*On leave from Institute of Isotopes, Hungarian Academy of Sciences, H-1525 Budapest, P.O.B. 77, Hungary.

†Author to whom correspondence should be addressed.

[1] *Chemical Designing and Processing of High-T_c Superconductors*, edited by M. Kawai and K. Kishio, special issue of Physica C **190** (1991).

[2] *Proceedings of the International Conference on Materials and Mechanisms of Superconductivity High-Temperature Superconductors III*, edited by M. Tachiki, Y. Muto, and Y. Syono, special issue of Physica C **185–190** (1991).

[3] *Proceedings of the International Conference on Materials and Mechanisms of Superconductivity High-Temperature Superconductors IV*, edited by P. Wyder, special issue of Physica C **235–240** (1994).

[4] *Crystal Engineering of High-T_c-Related Oxide Films*, edited by H. Koinuma, special issue of MRS Bull. **14** (1994).

[5] *Atomically Controlled Surfaces and Interfaces*, edited by M. Tsukada and A. Kawazu, special issue of Appl. Surf. Sci. **60-61** (1992).

[6] *Proceedings of the Second International Symposium of Atomically Controlled Surface and Interfaces*, edited by M. Lekela, special issue of Appl. Surf. Sci. **75** (1994).

[7] H. Koinuma and M. Yoshimoto, Appl. Surf. Sci. **75**, 308 (1994).

[8] H. Koinuma, H. Nagata, T. Tsukahara, S. Gonda, and M. Yoshimoto, Appl. Phys. Lett. **58**, 2027 (1991).

[9] M. Yoshimoto, H. Ohkubo, N. Kanda, H. Koinuma, K. Horiguchi, M. Kumagai, and K. Hirai, Appl. Phys. Lett. **61**, 2659 (1992).

[10] H. Tanaka, T. Matsumoto, T. Kawai, and S. Kawai, Jpn. J. Appl. Phys. **32**, 1405 (1993).

[11] T. Hikita, T. Hanada, M. Kudo, and M. Kawai, J. Vac. Sci. Technol. A **11**, 2649 (1993).

[12] Y. Liang and D. A. Bonnell, Surf. Sci. **285**, L510 (1993).

[13] M. Yoshimoto, T. Maeda, K. Shimozono, H. Koinuma, M. Shinohara, O. Ishiyama, and F. Ohtani, Appl. Phys. Lett. **65**, 3197 (1994).

[14] M. Kawasaki, K. Takahashi, T. Maeda, R. Tsuchiya, M. Shinohara, O. Ishiyama, T. Yonezawa, M. Yoshimoto, and H. Koinuma, Science **266**, 1540 (1994).

[15] H. Tabata, H. Tanaka, and T. Kawai, Appl. Phys. Lett. **65**, 1970 (1994).

[16] H. Tabata, H. Tanaka, T. Kawai, and M. Okuyama, Jpn. J. Appl. Phys. Part 1 **34**, 544 (1995).

[17] K. C. Mishra, K. H. Johnson, and P. C. Schmidt, J. Phys. Chem. Solids **54**, 237 (1993).

[18] W. Zhong, R. D. King-Smith, and D. Vanderbilt, Phys. Rev. Lett. **72**, 3618 (1994).

[19] R. D. King-Smith and D. Vanderbilt, Phys. Rev. B **49**, 5828 (1994).

[20] V. Ravikumar, D. Wolf, and V. P. Dravid, Phys. Rev. Lett. **74**, 960 (1995).

[21] M. Cherry, M. S. Islam, J. D. Gale, and C. R. A. Catlow, J. Phys. Chem. **99**, 14 614 (1995).

[22] W. Zhong and D. Vanderbilt, Phys. Rev. Lett. **74**, 2587 (1995).

[23] S. Kimura, J. Yamauchi, M. Tsukada, and S. Watanabe, Phys. Rev. B **51**, 11 049 (1995).

[24] M. J. Akhtar, Z. Akhtar, R. A. Jackson, and C. R. A. Catlow, J. Am. Ceram. Soc. **78**, 421 (1995).

[25] A. Miyamoto, T. Hattori, and T. Inui, Physica C **190**, 93 (1991).

[26] K. Kawamura, in *Molecular Dynamics Simulations*, edited by F. Yonezawa (Springer-Verlag, Berlin, 1992), p. 88.

[27] L. Verlet, Phys. Rev. **159**, 98 (1967).

[28] P. P. Ewald, Ann. Phys. (Leipzig) **64**, 253 (1921).

[29] M. Kubo, Y. Oumi, R. Miura, A. Fahmi, A. Stirling, A. Miyamoto, M. Kawasaki, M. Yoshimoto, and H. Koinuma, J. Chem. Phys. **107**, 4416 (1997).

[30] M. Kubo, Y. Oumi, R. Miura, A. Stirling, and A. Miyamoto, AIChE. J. (to be published).

[31] *Insight II User Guide Version 2.3.5* (Biosym Technol. Inc., San Diego, 1993).
[32] R. Miura, H. Yamano, R. Yamauchi, M. Katagiri, M. Kubo, R. Vetrivel, and A. Miyamoto, Catal. Today **23**, 409 (1995).
[33] R. W. G. Wyckoff, *Crystal Structure* (Wiley, New York, 1963), Vol. 1.
[34] K. Nassau and A. E. Miller, J. Cryst. Growth **91**, 373 (1988).
[35] R. J. Beals and R. L. Cook, J. Am. Ceram. Soc. **40**, 279 (1957).
[36] *Handbook of Chemistry and Physics*, 68th ed. (CRC, Boca Raton, 1987).
[37] E. N. Bunting, G. R. Shelton, and A. S. Creamer, J. Am. Ceram. Soc. **30**, 114 (1947).
[38] M. Kawasaki, M. Yoshimoto, and H. Koinuma (private communication).